HEAT TREATMENT AND CREEP CRACK GROWTH IN 9Cr–1Mo STEEL

JAROSLAV BALÍK[1]*, MILOŠ JANEČEK[2], JAN HAKL[1]

The crack growth rate in 9Cr-1Mo ferritic steel is measured at the upper expected service temperature 600 °C when the creep flow comes about. The samples of TDCB--type and mode of constant applied load are employed, the total test time ranging from ∼30 to ∼4500 h. In order to estimate a mechanical response to a prospective structural instability, two material variants differing in heat treatment are tested: normalized and tempered base metal and pre-aged material, which is the base metal subjected to long term static ageing before loading. Crack growth rates are presented in terms of load amplitude (parameter) C^*, as it is usual for creeping cracked body. The load amplitude is obtained by means of rates of plastic displacements in line of applied load, provided that the stress exponents of creep power law for respective materials are known. From the point of view of crack growth resistance, a structure degradation as a consequence of some exposure to high temperatures is revealed. It is suggested to relate this effect to grain boundary precipitation. Using scanning electron microscopy of fracture surfaces, the fracture mechanism that controls the crack growth is estimated. This process seems to be initiated by grain boundary cavitation and completed by joining of grain boundary microcracks with a possible contribution of void coalescence.

TEPELNÉ ZPRACOVÁNÍ A RŮST CREEPOVÉ TRHLINY V OCELI 9Cr–1Mo

Rychlost růstu trhliny ve feritické oceli 9Cr-1Mo je měřena při horní provozní teplotě 600 °C, kdy dochází ke creepové deformaci. Jsou užívány vzorky typu TDCB a režim konstantního vnějšího zatížení, přičemž celkové doby testu se pohybují od ∼30 do ∼4500 h. Pro posouzení mechanického účinku případné strukturní nestability jsou testovány dva materiály odlišně tepelně zpracované: normalizačně žíhaný a popuštěný základní kov a předžíhaný materiál, což je základní kov podrobený dlouhodobému statickému žíhání před zatížením. Rychlosti růstu jsou prezentovány jako závislé na amplitudě (parametru) zatížení C^*, jak je obvyklé pro těleso s trhlinou namáhané creepem. Amplituda zatížení je určena prostřednictvím rychlostí plastických posunutí podél přímky vnějšího zatížení, předpokládaje, že jsou známy exponenty creeepového mocninného zákona pro příslušné

[1] SVÚM, a.s., Research Centre Běchovice, 190 11 Praha 9, Czech Republic
[2] Department of Metal Physics, Charles University, Ke Karlovu 5, 121 16 Praha 2, Czech Republic
* corresponding author, e-mail: svum@mbox.vol.cz

materiály. Z hlediska odporu proti šíření trhliny byla zjištěna degradace struktury v důsledku určité vysokoteplotní expozice. Je navrženo přisoudit tento jev precipitaci v hranicích zrn. S užitím scanovací elektronové mikroskopie lomových ploch byl vyhodnocen lomový mechanismus, jenž řídí šíření trhliny. Zdá se, že tento proces je iniciován kavitací v hranicích zrn a ukončen spojením hraničních mikrotrhlin s možným příspěvkem koalescence dutinek.

K e y w o r d s: creep crack growth, structure degradation, precipitation, fracture mechanisms, fracture surfaces

1. Introduction

Ferritic steels of a standard composition of about 9Cr-1Mo offer a suitable combination of the engineering properties such as creep strength, ductility and corrosion resistance. That is why the steels of this kind are extensively used as materials for tubes, pipes and other components in steam generators and turbines in power plants and in chemical industry as well.

The lifetime of a structure or a part is given by the evolution of various types of damage which results in acceleration of macroscopic deformation and the final rupture of the component. The evolution of mesoscopically uniform damage of a structure may be related with familiar and widely performed creep tests of the respective material. Combining typical outputs of such tests, i.e. stationary plastic rates, stress exponents and times to rupture with the continuum mechanics of a finite body, the lifetime of a real structure may be assessed successfully. Yet, if the stability (free energy) conditions favour the rise and growth of cracks, these influence significantly and in a non trivial manner the rate of degradation of a part during its exposure to service loads.

Assuming the cracks development is allowed in a component made from a fairly ductile material, the lifetime may be qualitatively divided into two steps:

– The nucleation and the subcritical growth of cracks. Both macroscopic deformation (the deflection or displacement along the load line in the case of test samples) and crack length increase slowly enough so that the part may be kept in service. The uncracked ligament is yet not damaged substantially and remains in the material state similar to primary or secondary creep.

– Critical crack growth after a critical point is arrived. This regime nearly corresponds to spreading of tertiary creep stage on a more extended part of uncracked ligament. As the bearing cross section continues to diminish and the collapse conditions (at constant load) are approached, both crack growth and line displacement rates accelerate further which corresponds to catastrophic macroscopic deformation terminated by the component rupture.

According to that said above, after the crack is nucleated in a loaded creeping body, the remaining safe exploitation time is limited by the meeting the critical point. Hence, the most accurate information about subcritical crack growth rate

is necessary for the lifetime of a component to be estimated reliably. The primary aim of the present paper is to obtain data on creep crack growth in 9Cr-1Mo type steel at the upper expected service temperature, i.e., 600 ℃. We also attempt to test the effect of a prospective structural instability on the crack growth. For these purposes, not only the base metal, but also a long term pre-aged material are tested mechanically and compared using light and scanning electron microscopy.

2. Experimental

The steel investigated in our experiments was supplied by VITKOVICE steelworks as a forging of the composition (in weight %) 0.1 C, 0.43 Si, 0.4 Mn, 0.015 P, 0.006 S, 8.5 Cr, 0.88 Mo, 0.1 Ni, 0.23 V, 0.01 Al, 0.045 N. The base metal was prepared by normalization (austenitizing) ageing at (1065 ± 25) ℃ and air cooling, followed by tempering at (745 ± 15) ℃ and air recooling.

Mechanical examinations of crack growth were performed using the so called tapered double cantilever beam (TDCB) specimens of two shape forms, as shown in Fig. 1. All the samples were sidegrooved along the nominal plane of crack propagation to develop straight-fronted cracks and to support the plane strain character of loading mode I (normal tearing), if a tensile load P is applied according to Fig. 1. Test temperature was 600 ℃ and the loads, constant during each test, were chosen between (3900–15100) N yielding the initial stress intensity factors in the range of (18–58) $\mathrm{MN \cdot m^{-3/2}}$. In the specimen b) in Fig. 1, the stress intensity factor does not vary substantially within a fairly wide range of crack lengths.

Both load-free displacement along the line of applied force as well as the position of crack tip are evaluated using a microscope on the sample removed from

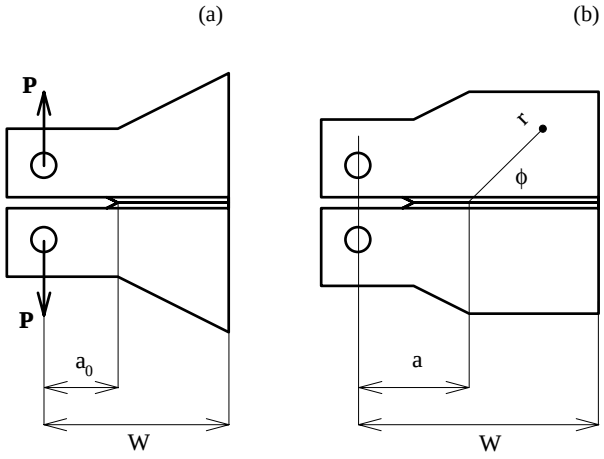

Fig. 1. TDCB samples: basic thickness 10 mm, thickness in sidegrooves 4 or 6 mm. a) $W = 50$ mm, b) $W = 65$ mm.

the furnace and these data are recorded together with the total time spent since the start of heating. Density of these measurements is determined by adjustable increment of total line displacement of the specimen.

In order to test the structure stability, a group of samples has been aged statically for the time 5000 h at 625 °C prior to mechanical testing. This thermal (load free) exposition was chosen to be comparable with long term tests, although owing to creep damage, a complete equivalence between loaded and load free states is obviously missing.

For mechanically tested specimens of both base and pre-aged materials, the microstructure was investigated optically, the etchant containing picric acid having been employed. The scanning electron microscopy (SEM) of fracture surfaces at various crack growth conditions was also carried out. Before it, the corrosion products were removed chemically using a hot solution of nitric acid and an ultrasonic cleaner.

3. Results

The light micrographs of base and pre-aged structures after their exposure to high temperature mechanical loading are presented in Figs. 2 and 3. As expected, the base material exhibits a tempered lath martensite structure in which a rather small number of fine precipitates may be observed. After the long term pre-aging, the basic structure features remain similar to the ones for non-aged material except for some rounding of grain edges, see Fig. 3. However, an appreciable coarsening

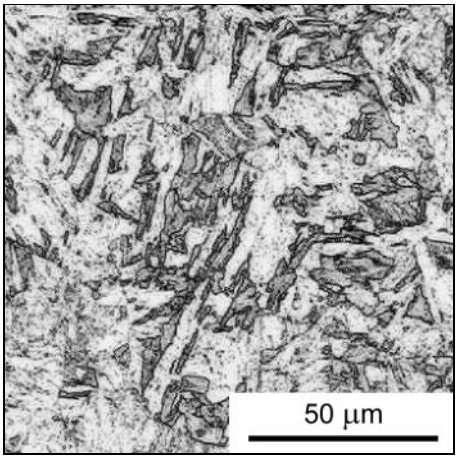

Fig. 2. Light micrograph of base material, exposed to crack growth test for 858 h at 600 °C.

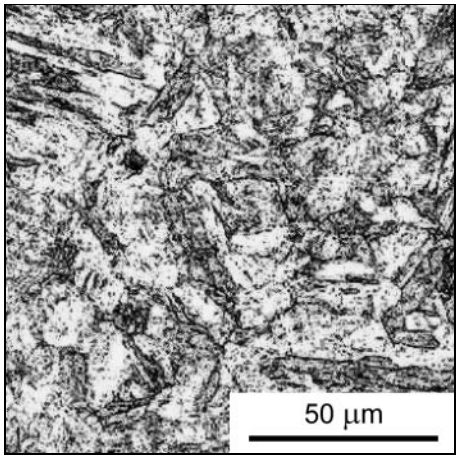

Fig. 3. Light micrograph of pre-aged material, exposed to crack growth test for 4490 h at 600 °C.

of precipitates and new precipitation at boundaries of grains and subgrains is observed. This agrees fully with the results [1] obtained for practically the same steel and similar heat treatment like in our case. In this work, the precipitates $[CrFe]_{23}C_6$ and Cr_2N are reported.

In order to treat the effect of general loading on crack growth in a real body, a proper driving force has to be chosen. Under this quantity, the stress tensor near the crack tip can obviously be assumed. Provided that methods for calculation of crack tip stresses are available, laboratory results as obtained on samples of specific geometries can be transferred on engineering components in principle.

Supposing a power-law viscous flow of our materials at high temperatures, the stress tensor near the crack tip in relation to two dimensional crack problem (HRR field) is given [2] by expression (in polar coordinates r, φ)

$$\sigma_{ij} = \left(\frac{C^*}{I_n A r}\right)^{\frac{1}{n+1}} \tilde{\sigma}_{ij}(\varphi). \tag{1}$$

Here A and n are the parameters of a power constitutive law

$$\dot{\varepsilon}_{ij} = \tfrac{3}{2} A s_{\mathrm{eq}}^{n-1} s_{ij} \tag{2}$$

with deviator of stress tensor, $s_{ij} = \sigma_{ij} - \frac{1}{3}\sigma_{kk}\delta_{ij}$, and equivalent tensile stress, $s_{\mathrm{eq}} = \sqrt{\frac{3}{2} s_{kl} s_{kl}}$. The Norton's creep law, $\dot{\varepsilon} = A\sigma^n$, is recovered as uniaxial form of (2). The dimensionless tensor $\tilde{\sigma}_{ij}$, that gives the dependence of stress components on polar angle, is normalized through the factor I_n for the maximum of $\tilde{\sigma}_{\mathrm{eq}}$ to equal unity. The scalar parameter C^* comprises all details of both sample geometry and external loading. Hence, it often plays an important role when the data about crack growth under conditions of viscous creep are reported and processed. For the present case of loading mode I, see Fig. 1, it can be written after [3] as

$$C^* = -\frac{1}{B}\frac{\partial U^*(a, \dot{\Delta})}{\partial a}, \tag{3}$$

where $\dot{\Delta}$ is the pure creep line displacement rate in the direction of load (i.e. at fixed crack length), B is the net specimen thickness between the sidegrooves, and U^* denotes the "power function" of the cracked body:

$$U^* = \int_0^{\dot{\Delta}} P(a, v)\mathrm{d}v. \tag{4}$$

When the mode of creep power law is extended on the whole bearing ligament, the line displacement rate can be written in terms of load as

$$\dot{\Delta} = k(a)P^n, \tag{5}$$

where k is the creep compliance of the cracked body. Using Eqs. (4) and (5), an experimentally appropriate expression for C^* follows:

$$C^* = \frac{P\dot{\Delta}}{(n+1)B}\frac{\mathrm{d}\lg k(a)}{\mathrm{d}a}. \tag{6}$$

In the next, the limit analysis approximation will be adopted [4], which is justified by the fact that $n \gg 1$. The load can be then expressed as a proportion of plastic collapse load, P_y

$$P \approx \psi\dot{\Delta}^{\frac{1}{n}}P_\mathrm{y}(a). \tag{7}$$

Provided the proportionality factor ψ depends only weakly on the crack length, Eqs. (5) and (7) yield the following approach:

$$\frac{\mathrm{d}\lg k(a)}{\mathrm{d}a} \approx -n\frac{\mathrm{d}\lg P_\mathrm{y}}{\mathrm{d}a} \equiv \frac{n}{W-a}\eta\left(\frac{a}{W}\right). \tag{8}$$

Accepting the plastic collapse load formula [5] for so called compact tensile samples (those are very similar to the ours)

$$\frac{P_\mathrm{y}}{\sigma_\mathrm{y}BW} = \frac{\sqrt{1-s\left[1-\left(\frac{a}{W}\right)^2\right]}+s\left(1-\frac{a}{W}\right)-1}{1-s},$$

the geometrical factor may be expressed as follows:

$$\eta\left(\frac{a}{W}\right) = 1+\frac{1}{\sqrt{1-s\left[1-\left(\frac{a}{W}\right)^2\right]}}. \tag{9}$$

Here σ_y is the yield stress, $s \doteq 0.6299$ and plane strain field in combination with Tresca's yield criterion are assumed. Substituting (8) in Eq. (6), the final formula for calculation of parameter C^* used here is

$$C^* = \frac{nP\dot{\Delta}}{(n+1)B}\frac{\eta\,(a/W)}{W-a}. \tag{10}$$

Note that according to the above derivation the expression (10) should be valid when the domain of stationary creep is fairly extended over the specimen. Some release of that restriction will be discussed later.

As to pure creep displacement rates appearing in (10), they will be identified with the ones derived from the as measured line displacements. Since the latter concern the load free state, no corrections regarding elastic deflections are necessary. The necessary stress exponent n has been drawn from published creep data [6] for base metal and from our conventional creep experiments for pre-aged material: $n = 13.2$ and $n = 12.8$, respectively. Both these values relate to 600 ℃.

Rather low density and large scatter of our data do not allow us to draw time derivatives of plastic line displacements and crack positions by common numerical procedures. Instead, we were forced to fit a suitable regression function to the whole data array and then to calculate the derivatives analytically. In the subcritical regime of crack growth, both distribution of data as well as theoretical considerations, see discussion, suggest a power time dependence of crack length. In order to involve the transition to the critical regime as well, we employed a regression function

$$a - a_0 = A_{\mathrm{a}} \frac{(t - t_0)^{\beta_{\mathrm{a}}}}{1 - \left(\dfrac{t}{T_{\mathrm{c}}}\right)^{m_{\mathrm{a}}}}, \tag{11}$$

where t_0 is time at which the crack growth starts to grow, T_{c} is the collapse time. A slightly generalised function has been used to fit the plastic line displacements:

$$\Delta = A_{\mathrm{u}} \frac{\left[1 + N(t - t_0)^{\beta_{\mathrm{u}}}\right]^{\frac{1}{N}} - 1}{1 - \left(\dfrac{t}{T_{\mathrm{c}}}\right)^{m_{\mathrm{u}}}} + \delta. \tag{12}$$

All the parameters appearing on the right-hand sides of (11) and (12), incl. the common quantities t_0 and T_{c}, are considered as regression coefficients. Examples of the respective fits to data are given in Fig. 4.

The maps of crack growth rate, as achieved by the above method, are presented in Figs. 5 and 6 for base and pre-aged materials, respectively. It is obvious from these plots, that there exists an asymptotic power-law relation between crack growth rate and load amplitude irrespective of whether the base material or the pre-aged one are concerned. In the case of pre-aged material, this limit behaviour appears if the test times are long enough, the respective onset time depending on the applied load and/or collapse time. Transient "tails" preceeding the asymptotic law, if any, are most often of concave type (yet also of convex type for the longest test). On the other hand, the general asymptotic behaviour has been detected in the base material only when the collapse time exceeded approximately 100 h. (This value

has been taken from the upward bent of the nose shaped curve concerning collapse time of 275 h, see Fig. 5.) For tests of shorter collapse times, a significant distinction appears: whereas the power law relation remains similar to that for long term tests, the level of growth rates is reduced by about one order of magnitude in comparison to the general asymptotic values for the same C^*.

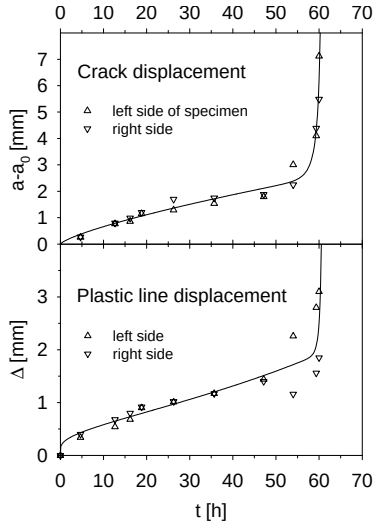

Fig. 4. Fit of regression functions (11), (12) to displacement data. Pre-aged material, sample $W = 50$ mm, load 10153 N, test temperature 600 °C.

4. Discussion

In viscous materials, the mechanism by which cracks grow involves as a rule nucleation, growth and coalescence of cavities ahead of the main crack tip. Supposing that achievement of a critical strain, ε_{f}, is a necessary condition for cavity coalescence and consequently for the failure, an approximate yet representative formula for crack growth rate is available [7]

$$\dot{a} \propto \frac{1}{\varepsilon_{\mathrm{f}}}[A(a-a_0)]^{1/(n+1)}[C(t)]^{n/(n+1)}. \tag{13}$$

Here, the assumption is incorporated that crack displacements $a-a_0$ are large enough as compared to a typical cavity spacing, x_{c}. The time dependent load amplitude $C(t)$, which is used instead of a more common quantity C^*, determines the time sequence of viscous fields of type (1) while the creep zone is spreading from a region close to the crack tip (small scale creep) to the whole specimen (extended creep). Thus, the relation (13) is suitable to involve effects of the initial elastic transients on crack growth in viscous materials, assuming that the viscous mode reaches very close to the crack tip, say, on the distance of length step x_{c} of fracture process.

The transient amplitude $C(t)$ for the small scale viscous field can be expressed by an appropriate interpolation formula [8] connecting viscous fields for short time and long time limits:

$$C(t) = C^* + \frac{\kappa K_{\mathrm{I}}^2}{(n+1)Et}, \tag{14}$$

where C^* is the amplitude for extended creep, K_{I} is initial stress intensity factor of an elastic field which determines both initial and remote boundary conditions for the small scale creep flow, $\kappa = 1$ or $1-\nu^2$ for plane stress or plane strain state,

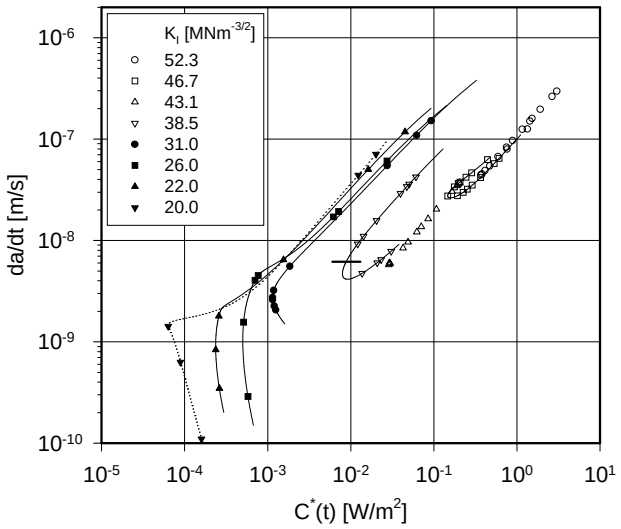

Fig. 5. Diagram of crack growth rate for base material. Slow growth for higher loads, i.e. short term tests; limit growth for lower loads, i.e. long term tests. Point of 100 h shown for the test $K_{\mathrm{I}} = 38.5\ \mathrm{MN \cdot m^{-3/2}}$ (initial value), $T_{\mathrm{c}} = 275$ h. Initial stress intensity factors are indicated.

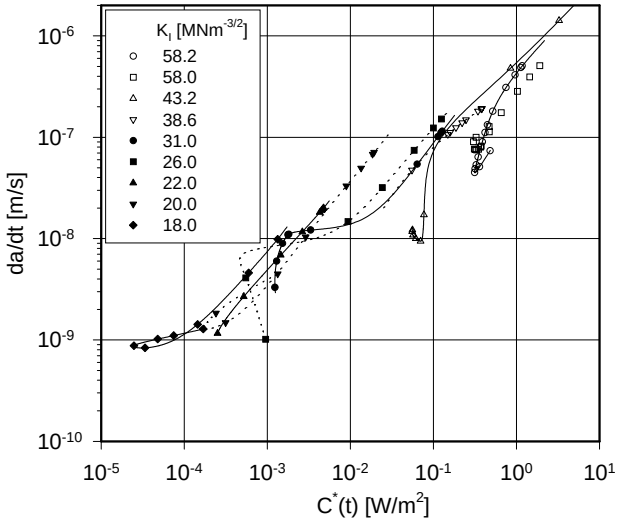

Fig. 6. Diagram of crack growth for pre-aged material. A common limit behaviour preceded by transients. Initial stress intensity factors are indicated.

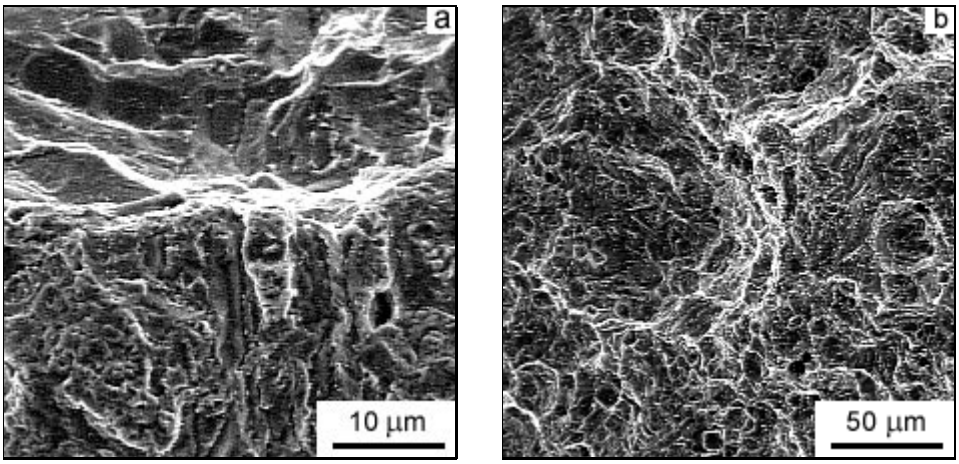

Fig. 7. SEM of fracture surfaces in base material after crack growth by medium rate at 600 °C. Sample $W = 65$ mm, $K_{\mathrm{I}} = 31$ MN·m$^{-3/2}$, $T_{\mathrm{c}} = 858$ h, crack propagation upward.

respectively, ν and E have their usual elastic meaning. One should note that in the literature several estimates of the transient load amplitude are referred [9], [10], which differ slightly from the expression (14). However, for the present specimen geometry, the exact transient amplitude can be well replaced [11] by the quantity $C^*(t)$ as calculated according to expressions (9, 10), provided that the respective transient displacement rates are inserted. Consequently, the experimental growth rate curves given in Figs. 5, 6 should be interpreted in terms of the growth rate expression (13), except perhaps for very early stage of crack development.

According to above considerations, straight segments of the rate curves in experimental maps $\dot{a}$ versus C^* involve not only extended creep mode, but also a substantial portion of small scale creep stage. The straight segments commence sometimes with a "turn points" separating decreasing and increasing segments of the same slope, see e.g. highest load curves in Figs. 5, 6. This is an obvious manifestation of transient behaviour, the possible effect of the factor $(a-a_0)^{1/(n+1)}$ being negligible already at the first recorded data. In very early stages of transients, as long as the zone of extensive creep damage remains small enough, the crack rates are significantly reduced with respect to back extrapolated power law, see concave tails on rate curves. This behaviour can be qualitatively related to the factor dependent on $a - a_0$ in expression (13), however, the underlying assumption of large crack increments disables the relation (13) to account for exactly the start of growth. According to [2, 4], for materials with $n \approx 10$, the initial growth rate is expected to be about one order of magnitude lower that the power-law value.

As it is manifested by Eq. (13), both creep flow as well as actual failure mech-

anism determine, through the respective parameters, the crack growth rate. In order to specify the fracture process, the scanning electron microscopy of the surface swept by the crack at various load levels and for both base as well as pre-aged material has been performed.

Examples of SEM micrographs for base material after high temperature exposition at medium load are shown in Fig. 7. A more detailed view, see Fig. 7a, reveals several stages of grain boundary damage. Grain boundary sliding of various extent and even intergranullar decohesion along facets out of the main crack surface may be distinguished. At an overwiev micrograph, see Fig. 7b, the fracture surface exhibits a typical dimpled intergranullar structure, although the details are perhaps poorer in comparison to those known from uniaxed experiments focused on failure. The reason is probably the chemical removal of the corrosion products, which was made before scanning. Since the similar features of fracture surface appeared at all investigated circumstances, a suggestion is implied to identify the present fracture mechanism with the well known (creep) grain boundary cavitation which is a mechanism typical for creep resistant materials at lower loads and elevated temperatures. It comprises nucleation of cavities at particles of second phase in grain boundaries, the growth and the coalescence of these cavities till grain boundary microcracks are formed, and finally the joining of microcracks that is synonymous with failure.

As to cavity growth rate relates, a model of constrained diffusive growth [12], in which a cavitating grain boundary surrounded by creeping matrix is considered, seems to be the most appropriate. In the case of uniaxial loading, the time to cavity coalescence on isolated boundary facet may be written [2]

$$t_{\mathrm{c}} \doteq 0.44 \left(\frac{1 + \dfrac{3}{n}}{\dot{\varepsilon}^2 d^2 J^*} \right)^{\frac{1}{3}} , \tag{15}$$

where J^* is the nucleation rate of cavities per unit grain boundary area, d is size of the cavitating facet and $\dot{\varepsilon}$ is the strain rate far from it. Only little information about the nucleation rate is still available. An empirical proportionality to strain rate [13] is commonly referred as

$$J^* = \alpha' \dot{\varepsilon}, \tag{16}$$

corresponding probably to favourable effect of strain induced vacancies and grain boundary sliding on cavity nucleation. In the present case of grain boundary cavitation, the factor α' can be assumed to increase (linearly?) with the grain boundary

concentration c_{gbp} of second phase particles. Consequently, the strain to rupture or more precisely Monkman-Grant product reads

$$\varepsilon_{\mathrm{f}} \equiv t_{\mathrm{c}}\dot{\varepsilon} = 0.44\frac{1+\dfrac{3}{n}}{d^2\alpha'(c_{\mathrm{gbp}})}. \tag{17}$$

The inverse proportionality between strain to fracture and grain boundary concentration of second-phase particles, see Eq. (17), may serve to reasoning of the previously mentioned difference in creep crack growth rate as dependent on thermal exposition. As long as the number of grain boundary particles remains low, a higher fracture strain is attained and, according to Eq. (13), a low crack growth rate follows. On the contrary, an enhanced precipitation on grain boundaries leads to a decrease of crack growth resistance, irrespective of whether due to static pre-aging or caused by high temperature mechanical loading. This way, the limit behaviour as defined for base and pre-aged materials in Figs. 5 and 6 should correspond to well developed (quasi saturated) precipitation. The precipitation represents a kind of structure degradation, therefore, with respect to the crack propagation. A similar role of grain boundary carbides in fracture process has been reported [14] for an austenitic steel as well.

For the pre-aged material, the fracture surfaces as revealed after the slowest and fastest crack passage are shown in Figs. 8 and 9, respectively. The value of crack growth rate does not affect noticeably the detailed view of the fracture surfaces,

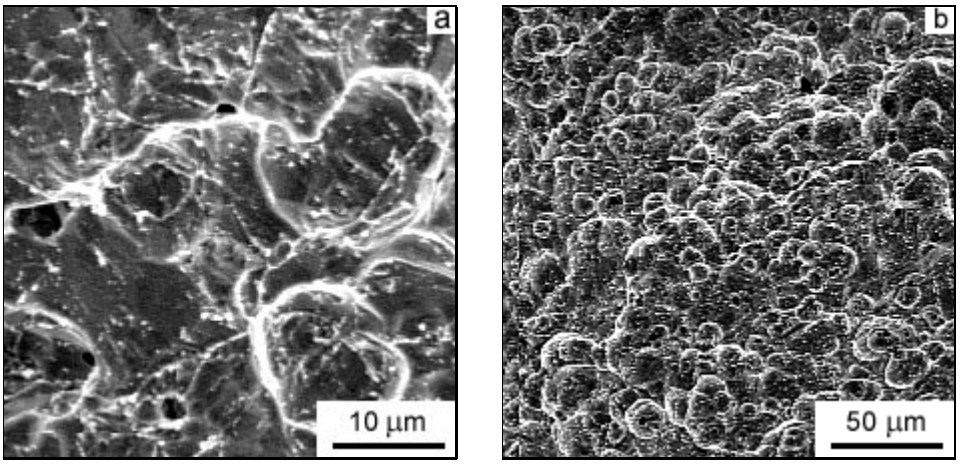

Fig. 8. SEM of fracture surfaces in pre-aged material after slow crack passage at 600 °C. Sample $W = 65$ mm, $K_{\mathrm{I}} = 18.0$ MN·m$^{-3/2}$, $T_{\mathrm{c}} = 4490$ h, crack propagation upward.

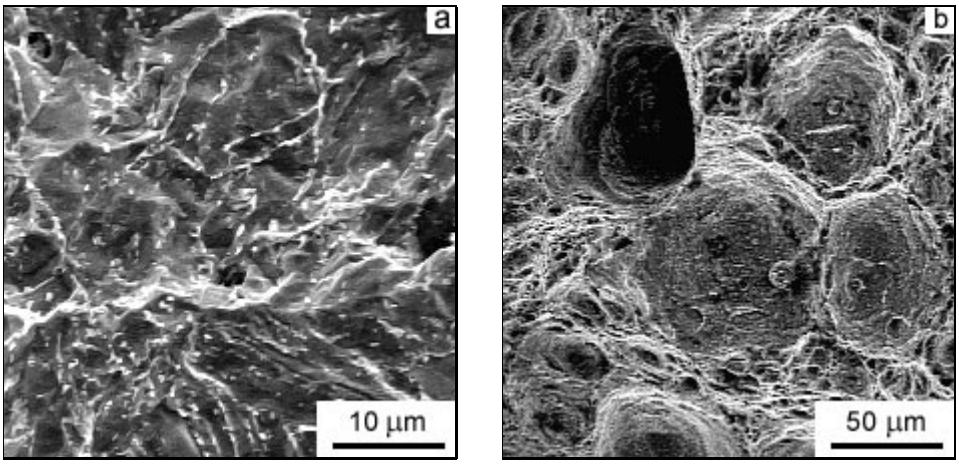

Fig. 9. SEM of fracture surfaces in pre-aged material after fast crack passage at 600 °C. Sample $W = 65$ mm, $K_I = 58.0$ MN·m$^{-3/2}$, $T_c = 45.2$ h, crack propagation upward.

cf. Figs. 8a and 9a. Except for rounded grain edges and appreciable precipitation, the depicted character of fracture surfaces is similar to the one observed in the base material, see Fig. 7a. Hence, the previously proposed fracture mechanism that proceeds by grain boundary cavitation and is completed by joining of grain boundary microcracks seems to be confirmed.

An attention will now be paid to a certain effect of the load level on the dimple morphology, see Figs. 8b, 9b. For low load (slow strain rates), the dimple structure is rather fine and regular, whereas at high load, a mixture of small and large dimples is observed, the latter controlling the failure probably. The appearance of large holes in the high stress state can result partly from an early nucleation at specific sites of the material, see Fig. 9b, partly from a rather high sensitivity of cavity growth rate to the stress concentration at those nucleation sites. Both these suppositions may be related to the superposition of dislocation creep flow and diffusion mechanism during cavity growth. The contribution of creep flow, the rate of which is highly stress sensitive, increases at high load and causes the first nucleated cavities at the sites of maximum stress concentration to develop extensively. For low load, on the contrary, the diffusion mechanism of much less stress sensitive rate not only dominates during cavity growth, but it can also relieve the stress singularities [14] prior the nucleation. Hence, a more regular and finer dimpled structure is developed.

5. Conclusions

– The data of creep crack growth in 9Cr-1Mo steel and at service temperature

600 ℃ were attained using TDCB – samples for both base metal as well as pre-aged material. The results of engineering importance are presented in plots of crack growth rate versus load parameter C^*.

– The significant suppression of limit growth rates is observed for less thermomechanically exposed base metal in comparison to the more exposed one and to the pre-aged material. An attempt is made to ascribe this effect to grain boundary precipitation during high temperature mechanical testing or static pre-ageing which results in enhanced nucleation rate of grain boundary cavities.

– The SEM of fracture surfaces seems to confirm the nucleation, growth and coalescence of grain boundary cavities as a mechanism governing the crack growth rate. The distribution of dimple sizes is influenced probably by the interplay between rates of diffusive and creep cavity growth as dependent on load.

Acknowledgements

We would like to dedicate the paper to Professor Dr. Z. Trojanová on the occasion of her 60^{th} birthday. This work was supported by the Grant Agency of the Czech Republic under Project No. 106/00/0545.

REFERENCES

[1] CHOUDARY, B. K.—BHANU SANKARA RAO, K.—MANNAN, S. L.: Trans. Indian Inst. Met., *53,* 2000, p. 203.
[2] RIEDEL, H.: Fracture at High Temperatures. Berlin, Springer-Verlag 1987.
[3] LANDES, J. D.—BENGLEY, J. A.: In: Mechanics of Crack Growth, ASTM STP 590, Philadelphia, American Society for Testing and Materials, 1976, p. 128.
[4] WEBSTER, G. A.: Mater. at High Temp., *10,* 1992, p. 74.
[5] MILLER, A. G.: Int. J. Press. Vess. Piping, *32,* 1988, p. 197.
[6] SKLENIČKA, V.—KUCHAŘOVÁ, K.—DLOUHÝ, A.—KREJČÍ, J.: In: Materials for Advanced Power Engineering 1994. Part I. (Proc. of a Conf. held in Liege, Belgium). Eds.: Coutsouradis, D. et al. Dordrecht, Kluver Academic Publishers 1994, p. 435.
[7] RIEDEL, H.: Fracture Mechanisms. In: Materials Science and Technology, *6.* Eds: Cahn, R. W. et al. VCH, Weinheim 1993.
[8] EHLERS, R.—RIEDEL, H.: In: Advances in Fracture Research. Proceedings of ICF5. Vol 2. Eds.: Francois, D. et al. Oxford, Pergamon Press 1981, p. 691.
[9] SAXENA, A.: In: Fracture Mechanics: 17th Symposium, ASTM STP 905. Eds.: Underwood, J. H. et al. Philadelphia, American Society for Testing and Materials, 1986, p. 185.
[10] AINSWORTH, R. A.: Mater. at High Temp., *10,* 1992, p. 119.
[11] SAXENA, A.: Mater. at High Temp., *10,* 1992, p. 79.
[12] RICE, J. R.: Acta Metall., *29,* 1981, p. 675.
[13] DYSON, B. F.: Scripta Metall., *17,* 1983, p. 31.
[14] BLACH, J.: Kovove Mater., *38,* 2000, p. 315.
[15] ARGON, A. S.—CHEN, I. W.—LAU, C. W.: In: Three-Dimensional Constitutive Equations and Ductile Fracture. Ed.: Nemat-Nasser, S. Amsterdam, North-Holland Publishing Company 1981, p. 23.

Received: 5.6.2002